JOURNAL OF COMPUTATIONAL PHYSICS 23, 200–217 (1977)

Evaluation of Phase-space Volumes and Inclusive Spectra in the Uncorrelated Jet Model

J. ENGELS AND J. FLEISCHER

Department of Theoretical Physics, University of Bielefeld, Germany

Received June 3, 1976; revised July 22, 1976

A new way to evaluate phase-space volumes and inclusive spectra in the uncorrelated jet model is studied in detail and compared to the well-known Monte Carlo and saddle point techniques. The method is based on Fourier transformation of the phase-space volumes. Apart from the very low-energy region, where only phase spaces with two, three, or four particles contribute, the new method is superior in accuracy and/or computing time to all other methods. As an application we study the approach of the normalized x and y single-particle distributions to their respective scaling limits.

1. INTRODUCTION

In this paper we present a method[1] for the accurate calculation at nonasymptotic energies of the transverse-momentum cutoff phase-space volume $\Omega(q)$ and of inclusive quantities, especially single-particle distributions, connected to $\Omega(q)$ in the uncorrelated jet model (UJM) [2–4].

This model is of interest in all kinds of multiparticle production processes, where the single events are assumed to have jet structure. In the UJM the fully exclusive distribution for the production of N particles of four-momentum p_i is given by

$$\Gamma_N \sim \frac{\kappa^N}{N!}\,\delta^{(4)}\left(\sum_{j=1}^{N} p_j - q\right)\prod_{i=1}^{N}\frac{d^3p_i}{2p_{i0}}f(p_{iT}), \tag{1.1}$$

q is the total four-momentum of the system, $p_{iT} = (p_{ix}^2 + p_{iy}^2)^{1/2}$, i.e., we choose the z-direction to coincide with the jet axis. For simplicity we assume that all particles have the same mass. The function $f(p_T)$ describes the transverse-momentum cutoff. In our numerical examples and the formulas we used

$$f(p_T) = \exp[-\lambda p_T], \tag{1.2}$$

[1] After completion of the main part of our work we learned about a paper of J. Gasser [1], where in principal the same method is worked out. The two papers differ, however, in many respects: we use different integration methods, and whereas our calculations are checked against Monte Carlo and saddle point calculations and are done with $m = m_\pi$, the author of [1] made only a comparison to an asymptotic expression and used $m = 1$ GeV. Moreover, we calculate and check single-particle spectra, and are able to say where each method can be applied.

ISSN 0021-9991

although the method is also applicable for other functions $f(p_T)$ describing a cutoff. The transversely cutoff phase-space volume is then given by

$$\Omega(q) = \sum_{N=2}^{\infty} \frac{\kappa^N}{N!} \int \prod_{i=1}^{N} \frac{d^3p_i}{2p_{i0}} e^{-\lambda p_{iT}} \delta^{(4)}\left(\sum_{j=1}^{N} p_j - q\right)$$
$$= \sum_{N=2}^{\infty} \frac{\kappa^N}{N!} \Omega_N(q) \tag{1.3}$$

and the normalized single-particle distribution is

$$F(Q, \mathbf{p}) \equiv \frac{2p_0}{\sigma_{\text{tot}}} \frac{d^3\sigma}{d^3p} = \kappa \exp(-\lambda p_T) \frac{\Omega(Q - p)}{\Omega(Q)}, \tag{1.4}$$

where $Q = (s^{1/2}, \mathbf{0})$. In principle all other inclusive quantities, e.g., two-particle correlations can be obtained in a similar way from $\Omega(q)$.

There are essentially three possibilities to evaluate $\Omega(q)$ or $\Omega_N(q)$.

(i) *The Monte Carlo method.* Provided one has enough computer time, one can calculate each $\Omega_N(q)$ with arbitrary precision [5]. The derivative with respect to any function of the integration variables can easily be performed; however, since the total number of events is then distributed over many bins, an essential loss in precision compared to the one for $\Omega_N(q)$ cannot be avoided. The calculation of second- and higher-order derivatives, e.g., for invariant single- or two-particle cross sections, is, then (because there is too little computer time) in practice not feasible. At high energies, where more and more states with higher multiplicities can contribute to inclusive quantities, the whole procedure becomes clumsy, since the results for many different Ω_N have to be calculated separately and added up. Also, a deviation of the cutoff function $f(p_T)$ from the one for which the importance sampling originally was done ($f(p_T) = \exp(-\lambda p_T^2)$ in [6]) decreases the statistics for high energies.

(ii) *Saddle point techniques and related statistical methods.* The formula for $\Omega_N(q)$ [7] consists in an expansion in powers of $1/N^{1/2}$ and is therefore most appropriate for big N values. To find the saddle point for general q-vectors one has to solve two nonlinear coupled equations, which reduce to one equation if $q_T = 0$. Usually, even for values $q_T \neq 0$ this procedure is adopted and subsequently one attaches a correction factor to the result. The method is therefore good for calculating Ω_N ($q = Q$), $\langle N \rangle$, f_2 and f_3 at not too small values of $s^{1/2}$ ($s^{1/2} > 3$ GeV for pions). It is very fast on the computer; however, at small energies it is bad because the low N-values dominate and it is inappropriate for the calculation of single-particle spectra because of its deficiencies in calculating phase-space volumes with $q_T \neq 0$.

(iii) *The Fourier transform method.* This method consists in evaluating a three-dimensional integral, which is obtained by Fourier transforming $\Omega(q)$ or $\Omega_N(q)$ and subsequent inverse transformation. For given $f(p_T)$ the first integral has to be done only once for all q; then a twofold integration remains, which can be calculated at nonasymptotic as well as asymptotic energies, with great accuracy and taking little

computer time. However, when phase spaces for $N = 2$, 3, or 4 dominate one should go back to Monte Carlo methods.

In Section 2 we shall describe the Fourier transform method in detail, as well as the numerical means to evaluate the integrals. The results for $\Omega(q)$ as well as for single-particle distributions will be compared to the ones obtained from methods (i) and (ii) in Section 3.

2. The Fourier Transform Method

The basic equations of the Fourier transform method have been derived by Bassetto, Sertorio, and Toller [3]. The main purpose of their own and other [4] treatments was to obtain asymptotic expansions for $\Omega(q)$, the single-particle distributions, etc., whereas we want to evaluate these equations numerically for finite, nonasymptotic values of the variables.

Consider the Fourier transform

$$Z(\beta) = \int d^4q \exp[i\beta q]\, \Omega(q) \tag{2.1}$$

and the transform of the single-particle phase-space volume

$$\begin{aligned} z(\beta) &= \int d^4q \exp[i\beta q]\, \Omega_1(q) \\ &= \int (d^3p/2p_0) \exp[i\beta p - \lambda p_T]; \end{aligned} \tag{2.2}$$

then, because of Eq. (1.3),

$$Z(\beta) = \sum_{N=2}^{\infty} (\kappa^N/N!)\, z^N(\beta) = \exp(\kappa z(\beta)) - \kappa z(\beta) - 1. \tag{2.3}$$

As a consequence of Lorentz invariance $\Omega(q)$ depends only on the two variables $q_E = (q_0^2 - q_L^2)^{1/2}$ and q_T, where $q_L = q_Z$ and $q_T = (q_x^2 + q_y^2)^{1/2}$ are the total longitudinal and transverse momenta, and we have chosen the z axis so that it coincides with the jet axis. Correspondingly, $Z(\beta)$ also depends on two variables $\beta_E = i\alpha_E$ and β_T only. Equations (2.1) and (2.2) can then be written as

$$Z(\beta) = 4\pi \int_0^\infty dq_T\, q_T J_0(\beta_T q_T) \int_0^\infty dq_E\, q_E K_0(\alpha_E q_E)\, \Omega(q) \tag{2.4}$$

and

$$z(\beta) = 2\pi \int_0^\infty dp\, p J_0(\beta_T p)\, K_0(\alpha_E(p^2 + m^2)^{1/2}) \exp(-\lambda p). \tag{2.5}$$

The inverse of the transformation Eq. (2.4) is given by

$$\Omega(q) = (1/4\pi^2 i) \int_{\epsilon - i\infty}^{\epsilon + i\infty} d\alpha_E\, \alpha_E I_0(\alpha_E q_E) \int_0^\infty d\beta_T\, \beta_T J_0(\beta_T q_T)\, Z(\beta). \tag{2.6}$$

As can be seen from Eqs. (2.3), (2.5), and (2.6) the numerical problem consists in the evaluation of a three-dimensional integral with highly oscillating complex integrands.

For $q = Q$ the β_T integrand is less varying, since $J_0(0) = 1$, and therefore

$$\Omega(Q) = (1/4\pi^2 i) \int_{\epsilon - i\infty}^{\epsilon + i\infty} d\alpha_E \, \alpha_E I_0(\alpha_E s^{1/2}) \int_0^\infty d\beta_T \, \beta_T Z(\beta). \tag{2.7}$$

On the other hand it is clear that large q_T, because of the factor $J_0(\beta_T q_T)$, will lead to numerical instabilities.

The first step in the computation of the integrals (2.5) and (2.6) is of course to find out for what values of the integration variables one should expect the main contributions. The integration path which is chosen for the α_E integration and the parameters involved, namely the mass m, the cutoff parameter λ, and the constant κ will play a role in this context. To be definite, we take in all calculations

$$m = m_\pi, \qquad \lambda = 6.2 \text{ (GeV)}^{-1}, \qquad \kappa = 36 \text{ (GeV)}^{-2} \tag{2.8}$$

in agreement with the values chosen in [4]. We are free to shift the integration path in the complex α_E plane to the right, the only singularity of the integrand being at $\alpha_E = 0$, namely, the logarithm contained in the K_0 function of Eq. (2.5). The path we choose is parallel to the imaginary axis, i.e., we take a fixed $\text{Re}\,\alpha_E = \epsilon > 0$. Notice that, because the integrand is a real analytic function in α_E for $\text{Re}\,\alpha_E > 0$, one has to consider only that part of the integration path which is in the upper half plane. The phase-space volume $\Omega(q)$ is then

$$\Omega(q) = \text{Re}\left\{\frac{1}{2\pi^2 i} \int_{\epsilon + i0}^{\epsilon + i\infty} d\alpha_E \, \alpha_E I_0(\alpha_E q_E) \int_0^\infty d\beta_T \, \beta_T J_0(\beta_T q_T) \, Z(\beta)\right\}. \tag{2.9}$$

We have calculated $\Omega(Q)$ for $1 \text{ GeV} \leqslant s^{1/2} \leqslant 20 \text{ GeV}$ with $\epsilon = 0.1$ and 1.0 (GeV)^{-1}. While we get good agreement with other calculations (see also Section 3) for $\epsilon = 0.1 \text{ (GeV)}^{-1}$, it seems to be impossible to get a reasonable result—at least with the same effort—for $\epsilon = 1.0 \text{ (GeV)}^{-1}$. In the following all calculations were therefore done with $\epsilon = 0.1 \text{ (GeV)}^{-1}$.

In Figs. 1a and b we show the β_T integrand,

$$G(\beta_T) = \beta_T J_0(\beta_T q_T) Z(\beta_T, \alpha_E) t(\beta_T) \tag{2.10}$$

for several α_E and q_T values, where

$$t(\beta_T) = (1 + \beta_T)^2 \tag{2.11}$$

is the Jacobian of the transformation $\beta_T = x/(1 - x)$ of the interval $0 \leqslant \beta_T \leqslant \infty$ to $0 \leqslant x \leqslant 1$. It is evident from these curves that up to $\beta_T = 30 \text{ (GeV)}^{-1}$ the integrand is nonnegligible. The α_E values were chosen from that α_E range, which is important for the α_E integration. The α_E integrand is shown in Fig. 2 for $q_E = 1$, 3, and 20 GeV and several q_T values. As expected from the singular behavior at $\alpha_E = 0$, the integrand is a rapidly decreasing function of $Im\alpha_E$, which is completely negligible above

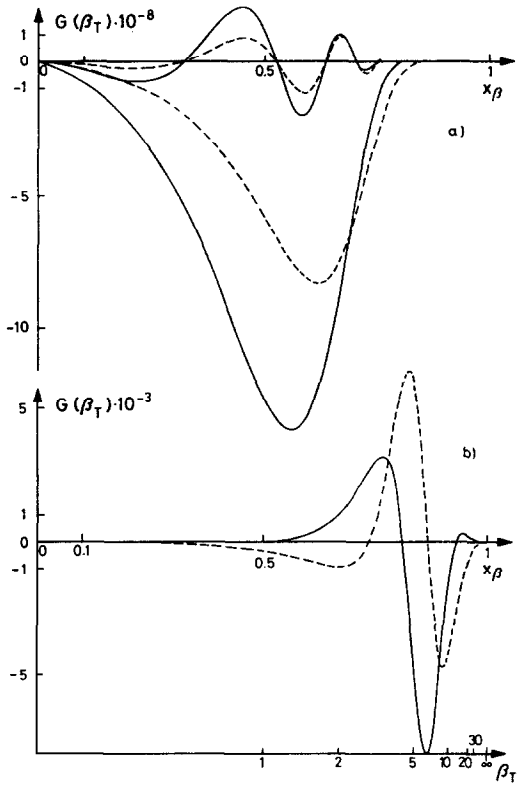

FIG. 1. The real part (solid lines) and the imaginary part (broken lines) of the β_T integrand $G(\beta_T)$, Eq. (2.10); (a) at $\alpha_E = (0.1 + i0.052)$ (GeV)$^{-1}$ and $q_T = 0$ and 5 GeV; (b) at $\alpha_E = (0.1 + i1.477)$ (GeV)$^{-1}$ and $q_T = 0$.

$Im\alpha_E = 2$ (GeV)$^{-1}$. Moreover, one recognizes that it is easy to obtain an accurate result for high q_E, whereas for low q_E ($q_E < 3$ GeV) the large positive and negative areas essentially cancel out, so that small inaccuracies in the integrand can spoil the result of the integration. Cancellations must occur, because as a consequence of four-momentum conservation only states with

$$Nm \leqslant (q^2)^{1/2} \tag{2.12}$$

can contribute. For $(q^2)^{1/2} < 2$ GeV one can circumvent this difficulty by taking in Eq. (2.3) a sum which is limited by the maximally allowed $N = N_{MAX}$ instead of the full exponential. The procedure is not useful for $(q^2)^{1/2} > 2$ GeV. We have made a test with Ω ($s^{1/2} = 3$ GeV) where $N_{MAX} = 21$ and found no difference in the two cases, whereas at $s^{1/2} = 1$ GeV ($N_{MAX} = 7$) the limited sum leads to much better results. With increasing N the calculation of the finite sum increases, however, the necessary computer time is considerable compared to that needed for the calculation of the exponential.

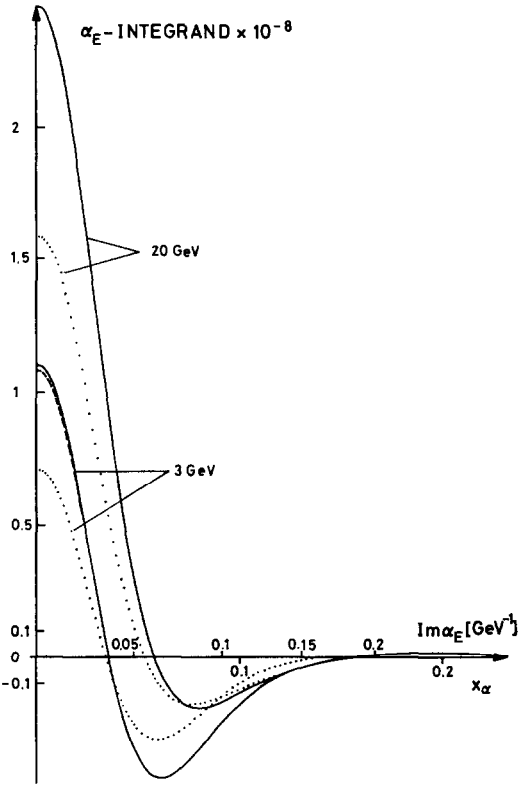

FIG. 2. The α_E integrand at $q_E = 3$ and 20 GeV for $q_T = 0$ (solid lines) and $q_T = 1$ GeV (dotted lines). The $q_E = 1$ GeV, $q_T = 0$ curve is a broken line; Re $\alpha_E = 0.1$ (GeV)$^{-1}$.

Being aware now of the relevant ranges in α_E and β_T we shall describe in the following the methods used to calculate the complex Bessel functions $I_0(W)$, $K_0(W)$, the quantity $z(\beta)$, and finally, $\Omega(q)$.

2.1. *The Bessel Functions $I_0(w)$ and $K_0(w)$*

Since we need the Bessel functions for complex arguments we cannot make use of the well-known standard programs. Instead we have programmed the ascending series [8]

$$K_0(w) = -\left[\ln\frac{w}{2} + \gamma\right] \cdot \sum_{n=0}^{\infty} \frac{(w^2/4)^n}{(n!)^2} + \sum_{n=1}^{\infty} \frac{(w^2/4)^n}{(n!)^2} \sum_{l=1}^{n} \frac{1}{l}, \tag{2.13}$$

$$I_0(w) = \sum_{n=0}^{\infty} \frac{(w^2/4)^n}{(n!)^2}, \tag{2.14}$$

where γ is the Euler constant, $\gamma = 0.577215...$, and the asymptotic expansions

$$K_0(w) \approx \left(\frac{\pi}{2w}\right)^{1/2} e^{-w} \left\{1 - \frac{1}{8w} + \frac{1 \cdot 9}{2!\,(8w)^2} - \frac{1 \cdot 9 \cdot 25}{3!\,(8w)^3} + \cdots\right\}, \tag{2.15}$$

valid for $|\arg w| < 3\pi/2$ and

$$I_0(w) \approx \frac{e^w}{(2\pi w)^{1/2}}\left\{1 + \frac{1}{8w} + \frac{1\cdot 9}{2!\,(8w)^2} + \frac{1\cdot 9\cdot 25}{3!\,(8w)^3} + \cdots\right\}, \tag{2.16}$$

valid for $|\arg w| < \pi/2$. With double precision variables (16 digits on the IBM 370/158 computer) and a required relative accuracy of 10^{-10} one has to change at $|w| \approx 9$–10 for $K_0(w)$ and at $|w| \approx 11$–12 for $I_0(w)$ from the small $|w|$ representations to the asymptotic expansions. At the matching point about 20–25 terms in the respective expansions have then to be calculated. A test for the $I_0(w)$ program was the relation

$$I_0(w) = J_0(iw), \qquad -\pi < \arg w \leqslant \pi/2. \tag{2.17}$$

It turns out that the asymptotic expansion Eq. (2.16) is inadequate near $\arg w \sim \pi/2$. We have therefore replaced Eq. (2.16) for $\pi/4 < \arg w \leqslant \pi/2$ by the corresponding asymptotic expansion for $J_0(w)$.

2.2. *The Fourier Transform z of the Single-particle Phase-space Volume*

The evaluation of Eq. (2.5) was performed using three methods:

(I) The application of the trapezoidal rule for $n_K = 2^K$ integration intervals to

$$z = -(2\pi/\lambda^2)\int_0^1 dx \ln x J_0(\beta_T' \ln x)\, K_0(\alpha_E'(\ln^2 x + m'^2)^{1/2}), \tag{2.18}$$

where $\alpha_E' = \alpha_E/\lambda$, $\beta_T' = \beta_T/\lambda$, and $m' = m\lambda$. The sequence of integrals z_K obtained for $K = 1,\ldots, 8$ was then used to accelerate the convergence of the integral with the Romberg method (see [9, 10] for a detailed description). This method corresponds to a polynomial extrapolation in h_K = subinterval length $= 1/n_K$ of the approximation z_K to the point $h_K = 0$.

(II) The same determination of the z_K as in I, but subsequent acceleration of the convergence of the integral with the ϵ algorithm [10], which is the application of Padé-approximants to the series

$$z(u) = z_1 + \sum_{j=1}^{\infty} (z_{j+1} - z_j)\, u^j \tag{2.19}$$

and its evaluation at $u = 1$. One starts with

$$\epsilon_{K,-1} = 0, \qquad \epsilon_{K0} = z_K \tag{2.20}$$

and then calculates

$$\epsilon_{Kl} = \epsilon_{K+1,l-2} + [\epsilon_{K+1,l-1} - \epsilon_{K,l-1}]^{-1}. \tag{2.21}$$

The resulting triangular table contains, for even 1 only, approximants to z which are diagonal Padé approximants for $K = 1$,

$$\epsilon_{1,2N} = [N, N]\,(u = 1); \tag{2.22}$$

whereas for $K = M - N + 1 > 1$,

$$\epsilon_{M-N+1,2N} = [N, M]\,(u = 1). \tag{2.23}$$

(III) Here we obtained the z_K from

$$z = (2\pi/\lambda^2)\int_0^\infty dp\, e^{-p} p J_0(\beta_T' p)\, K_0(\alpha_E'(p^2 + m'^2)^{1/2}) \tag{2.24}$$

using the Laguerre–Gauss integration method with $n_1 = 2$ and $n_K = 4 \cdot (K - 1)$ points for $K = 2,..., 11$ [11]. The method is especially designed for integrals over the range $(0, \infty)$ and a weight factor e^{-p}. Subsequently the ϵ algorithm was applied, if necessary.

Comparing the three methods, we can make the following statements.

(i) Even with 256 integration points the trapezoidal rule without acceleration will give a result which is true up to only the first two digits or worse, while for $Im\alpha_E < 2\ (\mathrm{GeV})^{-1}$, $\beta_T < 10\ (\mathrm{GeV})^{-1}$ the Laguerre–Gauss integration rule works with high precision, giving correctly the 8–10 leading digits for $n_K = 32$, 36 and 40 without acceleration.

TABLE I

$z(\alpha_E = (0.1 + i0.05)\ (\mathrm{GeV})^{-1}, \beta_T = 1.5\ (\mathrm{GeV})^{-1}); c = \lambda^2/2\pi$

K	$c\,\mathrm{Re}\, z_K^{\mathrm{III}}$	n_K	$c\,\mathrm{Re}\, z_K^{\mathrm{II}} = \epsilon_{K0}$	n_K	ϵ_{K2}	ϵ_{K4}	ϵ_{K6}
1	3.236243915...	2	1.386402167...	2	3.342440919...	3.221399969...	3.223869250...
2	3.216989326...	4	2.223255642...	4	3.273132212...	3.223444567...	3.223822864...
3	3.223684132...	8	2.702077489...	8	3.244970854...	3.223790558...	
4	3.223862718...	12	2.962520940...	16	3.233275622...	3.223820014...	
5	3.223779449...	16	3.098021271...	32	3.228233453...		
6	3.223769971...	20	3.165709885...	64	3.225965375...		
7	3.223772436...	24	3.198211711...	128			
8	3.223773654...	28	3.213182044...	256			
9	3.223773828...	32					
10	3.223773769...	36					
11	3.223773721...	40					

Best values and number of points used to obtain them

Method	n	cz
I	256	3.218955638 − i0.4234127367
II	256	3.223822865 − i0.4245001998
III	40	3.223773721 − i0.4244895469

(ii) The Romberg acceleration shifts the result in the right direction but normally does not even give the third digit correctly, whereas the ϵ algorithm brings 3 to 4 additional digits.

(iii) At the boundaries of the relevant α_E and β_T regions ($Im\alpha_E \approx 2$ (GeV)$^{-1}$, $\beta_T \approx 30$ (GeV)$^{-1}$) the z_K sequence obtained with the Laguerre–Gauss method does not seem to converge, while the z_K's from the trapezoidal rule do not oscillate very much around the true value z. Applying the ϵ algorithm to both sequences leads, however, to the same result for the first 3 to 4 digits.

In Table I we show the results for z at a typical point in the most relevant part of the ($Im\alpha_E$, β_T) plane. For small K the Laguerre–Gauss result is already better than that of method II, for which we show the ϵ-algorithm table. Table II contains the results for z at extreme $Im\alpha_E$ and β_T values, this time part of the ϵ-algorithm table belonging to Re z, and method III is displayed. As a consequence of our numerical experiments we adopted method III for the following calculations, taking $z = z_9$ ($\hat{=}$ 32 points) for $Im\alpha_E < 2$ (GeV)$^{-1}$, $\beta_T < 10$ (GeV)$^{-1}$ and performing the ϵ algorithm for larger β_T values on the sequence $z_1, \ldots, z_{11}$ ($\hat{=}$ 222 points). To give an impression of the function z we have drawn Figs. 3a and b.

TABLE II

$z(\alpha_E = (0.1 + i2)(\text{GeV})^{-1}, \beta_T = 30(\text{GeV})^{-1}); c = \lambda^2/2\pi$

K	$100c$ Re z_K^{II}	n_K	$100c$ Re $z_K^{III} = \epsilon_{K0}$	n_K	ϵ_{K6}	ϵ_{K8}	ϵ_{K10}
1	−13.309134142...	2	−8.906190943...	2	0.865125011...	1.446561195...	1.434069222...
2	5.050597081...	4	14.485811261...	4	1.465350474...	1.433341750...	
3	0.443955094...	8	−7.485913060...	8	1.433824807...	1.433638563...	
4	1.091066205...	16	3.764937754...	12	1.433267812...		
5	1.847716008...	32	2.935261600...	16	1.433703798...		
6	1.148064702...	64	−1.034031288...	20			
7	1.570435127...	128	3.723713731...	24			
8	1.385918052...	256	−0.315184860...	28			
9			2.629131290...	32			
10			0.678211632...	36			
11			1.882917526...	40			

Best values and number of points used to obtain them

Method	n	$100cz$
I	256	1.288686345 − i1.329409770
II	256	1.434676601 − i1.247092913
III	222	1.434069222 − i1.245043915

2.3. *The Phase-space Volume $\Omega(q)$*

The remaining two integrations of Eq. (2.9) have been attacked with five different methods.

(I) Direct application of the trapezoidal rule to the integrals without any transformation; the upper limit of the α_E integral was $\alpha_E = (0.1 + i2)$ (GeV)$^{-1}$ and that of the β_T integral was $\beta_T = 100$ (GeV)$^{-1}$.

(II) Two Legendre–Gauss integrations with 32 points each, the first by transforming the interval $[0, a]$ to $[-1, 1]$ with

$$y = (2/a)x - 1, \tag{2.25}$$

the second by transforming the interval $[a, \infty]$ to $[-1, 1]$ with

$$y = (x - 2a)/x, \tag{2.26}$$

where x was $Im\alpha_E$ or β_T and a was chosen to be 0.2 (GeV)$^{-1}$ for $Im\alpha_E$ and 2 (GeV)$^{-1}$ for β_T. At points with $Im\alpha_E > 2$ (GeV)$^{-1}$ or $\beta_T > 100$ (GeV)$^{-1}$ the integrand was set zero to avoid errors from possibly bad z values.

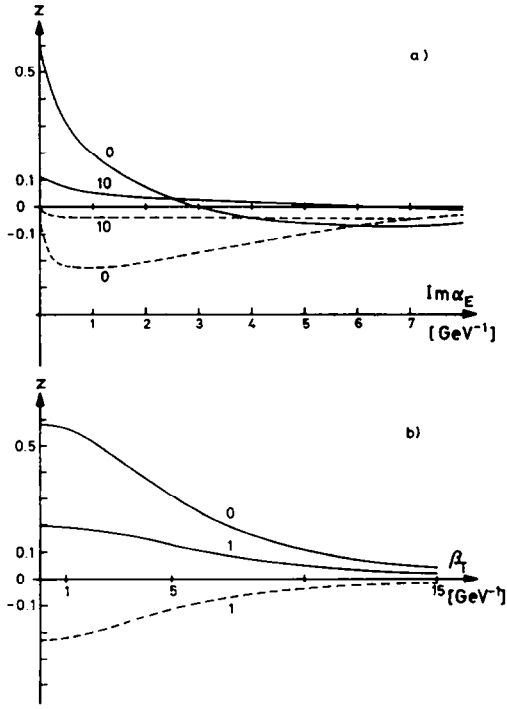

FIG. 3. The Fourier transform z of the single-particle phase-space volume, the real parts (solid lines) and imaginary parts (broken lines) are given for Re $\alpha_E = 0.1$ (GeV)$^{-1}$ in (a) at fixed $\beta_T = 0$, 10 (MeV)$^{-1}$, the numbers on the curves indicate the β_T values; (b) at fixed $Im\alpha_E = 0$, 1 (GeV)$^{-1}$, the numbers on the curves indicate the $Im\alpha_E$ values; the imaginary part for $Im\alpha_E = 0$ is zero.

(III) Transformation of the interval $[0, \infty]$ to $[0, 1]$ with

$$y(x) = x/(1 + x), \tag{2.27}$$

then trapezoidal integration in the y interval $[0, y(a)]$, where a was chosen to be 2 $(\text{GeV})^{-1}$ for $Im\alpha_E$ and ∞ $(\text{GeV})^{-1}$ for β_T. The integration intervals were divided into $n_K = 2^K$ $(K = 1,...,. 8)$ subintervals and the obtained sequences of integral approximations were accelerated with the Romberg or ϵ algorithms.

(IV) Laguerre–Gauss integration with $n_1 = 2$, $n_K = 4 \cdot (K - 1)$, $K = 2,..., 9$ points after a scale transformation $y = ax$ such that the highest x value was at the end of the relevant interval, i.e., $a = 2/111.7514$ for $Im\alpha_E$ and $a = 100/111.7514$ for β_T. The sequences of integral approximations were then accelerated via ϵ algorithm.

(V) Laguerre–Gauss integration with 64 points after a scale transformation similar to that in IV.

As a test we have calculated $\Omega(Q)$ for $s^{1/2} = 1$–20 GeV with all 5 methods. The resulting $\Omega(Q)$ agreed within less than 0.5 % for all $s^{1/2} \geqslant 5$ GeV with increasing

TABLE III

$\Omega(Q)$, $Q = (s^{1/2}, \mathbf{0})$, $\kappa = 36\ (\text{GeV})^{-2}$

	Method			
$s^{1/2}$ [GeV]	Fourier transform	Monte Carlo [4, 6]	Saddle point [7]	Three terms of asymptotic expansion [4]
1	2.509×10^2	2.495×10^2	1.088×10^2	
2	6.295×10^2		4.774×10^2	
3	1.388×10^3	1.292×10^2	1.159×10^3	
3.8	2.392×10^3	2.206×10^3	2.092×10^3	
4.8	4.316×10^3	3.933×10^3	3.860×10^3	
6	7.907×10^3		7.482×10^3	
7	1.228×10^4		1.192×10^4	
8	1.820×10^4		1.788×10^4	
9	2.596×10^4		2.569×10^4	
10	3.591×10^4		3.562×10^4	2.509×10^4
12	6.373×10^4		6.361×10^4	4.679×10^4
14	1.047×10^5		1.044×10^5	7.956×10^4
16	1.619×10^5		1.615×10^5	1.264×10^5
18	2.391×10^5		2.385×10^5	1.905×10^5
20	3.400×10^5	2.144×10^5	3.391×10^5	2.753×10^5

[2] The calculation of the 4096 z values for method II takes about $\frac{1}{2}$ hr on the IBM 370/158 computer.

agreement at higher energies (0.015 % at $s^{1/2} = 20$ GeV). Only method I differed a little more from the average values. A stronger test for the efficiency of the methods was the low-energy calculation of $\Omega(Q)$, especially at $s^{1/2} = 1$ GeV, where as explained already, strong cancellations occur and where we have, on the other hand, a rather accurate value for Ω from Monte Carlo calculations. With and without the finite sum trick, methods II and III lead to the best results. Although they are very different, methods II and III agree to less than 0.05 % in $\Omega(Q)$ for $s^{1/2} > 4$ GeV. Since method II requires only 4096 z values[2] compared to 65, 536 z values for method III, we have carried out all following calculations with method II. Because the z values are independent of q and κ it was only necessary to calculate them once and to store the result on tape. For fixed κ it is also worthwhile to store away $Z(\beta)$, since the evaluation of the complex double-precision exponential in Eq. (2.3) or the corresponding expansion takes considerable computer time.

3. Numerical Results

In Table III we have listed $\Omega(Q)$ for various values of $s^{1/2}$ between 1 and 20 GeV, calculated with our method, the Monte Carlo method [6], the saddle point technique [7], and the first three terms of the asymptotic expansion as given by Eq. (A.13) (divided by 4π) of [4]. As already explained in the introduction, the Monte Carlo calculation is the most reliable at low energies, whereas at high energies the asymptotic expansion (because of slow convergence with more than three terms) and/or the saddle point result should be taken for comparison. The Fourier transform method works well in both regions. This is also confirmed by the coincidence of the results obtained with different integration rules.

Another crucial point in the test of the methods is the calculation of $\Omega(q)$ with $q_T \neq 0$. As can be seen from Eq. (1.4) this is already needed in the simplest inclusive distribution, the single-particle distribution. Moreover, the single-particle distribution is of theoretical interest because of its asymptotic scaling properties in the UJM. We have, therefore, as a test and as an application, calculated the normalized x, p_T^2, p_L, y, and cos θ single-particle distributions. The connections of these distributions in the UJM to the invariant s.p.d. $F(Q, \mathbf{p})$ are

$$\frac{1}{\sigma_{tot}} \frac{d\sigma}{dx} = \pi s^{1/2} \int_0^{p_1(x)} dp_T \frac{p_T}{p_L} F, \tag{3.1}$$

with

$$x = \frac{2p_0}{s^{1/2}}, \qquad p_1(x) = p = \left(\frac{s}{4} x^2 - m^2\right)^{1/2}, \qquad p_1(1) \equiv p_{MAX}; \tag{3.2}$$

$$\frac{1}{\sigma_{tot}} \frac{d\sigma}{dp_T^2} = \frac{\pi}{2} s^{1/2} \int_{x_1(p_T^2)}^1 dx \frac{F}{p_L}, \tag{3.3}$$

with

$$x_1(p_T^2) = \left[\frac{4}{s}(p_T^2 + m^2)\right]^{1/2}; \tag{3.4}$$

$$\frac{1}{\sigma_{tot}}\frac{d\sigma}{dp_L} = \pi \int_0^{p_2(p_L)} dp_T \frac{p_T}{p_0} F, \tag{3.5}$$

with

$$p_2(p_L) = (p_{MAX}^2 - p_L^2)^{1/2}; \tag{3.6}$$

$$\frac{1}{\sigma_{tot}}\frac{d\sigma}{dy} = \pi \int_0^{p_3(y)} dp_T\, p_T F, \tag{3.7}$$

with

$$y = \frac{1}{2}\ln\frac{p_0 + p_L}{p_0 - p_L}, \qquad p_3(y) = \left(\frac{s}{4}\cosh^{-2} y - m^2\right)^{1/2}; \tag{3.8}$$

$$\frac{1}{\sigma_{tot}}\frac{d\sigma}{d\cos\theta} = \frac{\pi}{2} s^{1/2} \int_{x_0}^1 dx\, pF, \tag{3.9}$$

with

$$\cos\theta = \frac{p_L}{p}, \qquad x_0 = \frac{2m}{s^{1/2}} = x_1(0). \tag{3.10}$$

A further test was the evaluation of sum rules, e.g., for the x distribution

$$\int_{x_0}^1 \frac{dx}{\sigma_{tot}}\frac{d\sigma}{dx} = \langle N \rangle, \qquad \int_{x_0}^1 dx \frac{x}{\sigma_{tot}}\frac{d\sigma}{dx} = 2. \tag{3.11}$$

In the calculation of the distributions two points have to be considered: (i) Due to the factor $1/p_L$ the integrands belonging to the x and p_T^2 distributions each contain a square-root singularity at one end of the integration interval, since the invariant s.p.d. $F(Q, \mathbf{p})$ and $\Omega(Q\text{-}p)$ are *not* vanishing at the end of the physical region. The singularity is integrable.[3] (ii) The contribution to $F(Q, \mathbf{p})$ coming from the two-particle final state is proportional to a δ function and has to be added separately. It is negligible for $s^{1/2} > 3$ GeV, but important at smaller energies. Details are given in the Appendix.

The integrations in Eqs. (3.5), (3.7), (3.9), and the sum rules were performed with the Simpson rule. To obtain the integrals in Eqs. (3.1) and (3.3) the function F was interpolated in subintervals with parabolas so that the integration could be done analytically. The resulting x distributions were compared to corresponding Monte Carlo calculations at $s^{1/2} = 1, 3, 3.8, 4.8$, and 20 GeV taken from [4]. We got complete

[3] The singularity in the integrand of Eq. (3.1) could have been avoided by choosing p_L as the integration variable; however, because of the structure of Eq. (2.6) it is preferable for the numerical evaluation to take q_T as one of the two variables on which $\Omega(Q - q)$ depends.

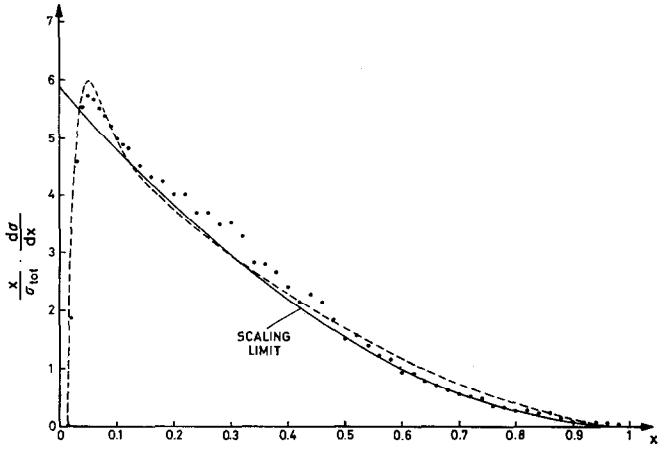

FIG. 4. The normalized single-particle x distribution multiplied by x at $s^{1/2} = 20$ GeV; the points are the result of a Monte Carlo calculation, the broken line is the Fourier transform method result. For comparison we show the scaling limit curve (solid line).

coincidence of the curves for $s^{1/2} = 3$, 3.8, and 4.8 GeV. At $s^{1/2} = 1$ GeV the two calculations agree well for $x \lesssim 0.5$; for bigger values, where only particle numbers for $N = 2$, 3, or 4 can contribute, the Fourier transform method (FTM) fails. In Fig. 4 we show the results of the two methods at 20 GeV. Clearly the FTM is superior over the Monte Carlo method (MCM) in this energy range in two respects: it is much more accurate and needs much less computation time (10 min for the FTM, 40 hr for the MCM on the IBM 370/158 computer). The additional sum rule tests work well, e.g., the energy sum rule in Eq. (3.11) is fulfilled to better than 0.5 % for $s^{1/2} \geqslant 3$ GeV and still to 1 % for $s^{1/2} = 2$ GeV. Remember that the energy sum rule is trivial for the

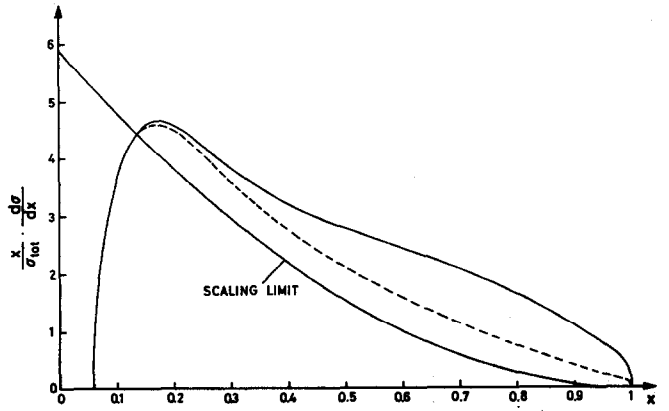

FIG. 5. The normalized single-particle x distribution multiplied by x at $s^{1/2} = 4.8$ GeV calculated with the saddle point method (solid line), with the Fourier transform method (broken line) and the scaling limit curve (solid line).

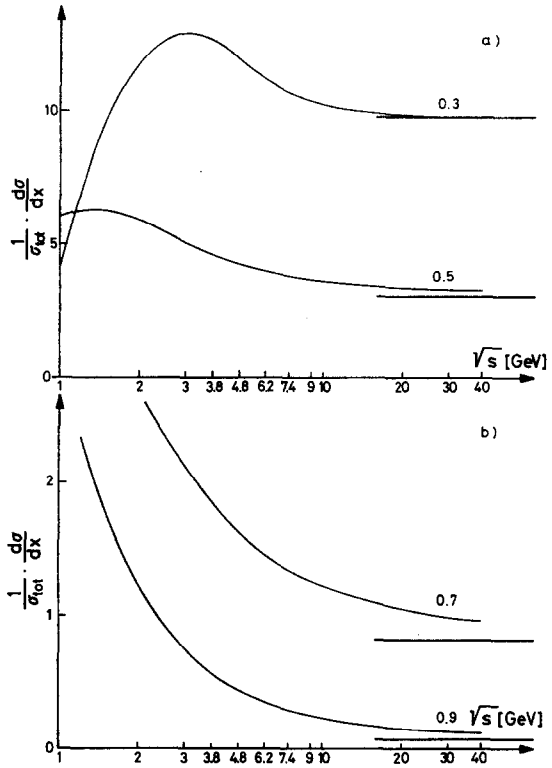

FIG. 6. The approach of $(1/\sigma_{tot})(d\sigma/dx)$ at fixed x values, indicated by the numbers on the curves, to the scaling limit value (fat solid line). The $s^{1/2}$ scales are logarithmic ones. (a) $x = 0.3$ and $x = 0.5$; (b) $x = 0.7$ and $x = 0.9$.

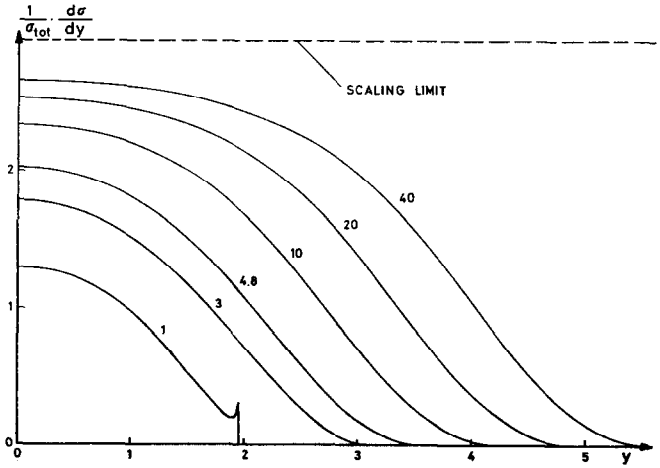

FIG. 7. The approach of $(1/\sigma_{tot})(d\sigma/dy)$ to the scaling limit (broken line). The numbers on the lines are the $s^{1/2}$ values in gigavolt units.

MCM, where each event conserves energy, but not for the FTM, where all points are calculated independently. We have also checked the saddle point method (SPM) by calculating the x distribution at $s^{1/2} = 4.8$ GeV. In Fig. 5 we show the SPM and FTM results. As already mentioned in the introduction, the difficulties with the $q_T \neq 0$ phase-space volumes in the SPM lead to a wrong single-particle spectrum—the energy sum rule has a 25 % error. To test the p_T^2, p_L, y, and $\cos\theta$ distributions we have produced the corresponding curves with the MCM and with the FTM. We find complete coincidence of the curves.

As an application we have studied the approach of the x and y-distributions to their corresponding scaling limits. For $x = 0.3$, 0.5, 0.7, and 0.9 we show in Figs. 6a and b the dependence of the x distribution on the total C.M.S. energy $s^{1/2}$ and the convergence to the limiting x distribution (see [4]). In Fig. 7 we give several y distributions for energies between 1 GeV and 40 GeV. The expected limiting plateau height $\tilde{\kappa} = \pi\kappa/\lambda^2$ (= 2.942 with our parameter values) is only slowly approached from below. So, the UJM, at least with the parameter values of (2.8), leads to a very late scaling of the normalized single-particle distribution.

4. Summary and Outlook

To summarize we can say the following about the Fourier transform method:

(i) For the calculation of inclusive quantities in the uncorrelated jet model, like $\Omega(q)$ and single-particle spectra, if $s^{1/2} \gtrsim 2$ GeV the FTM is superior in accuracy and/or computing time to the Monte Carlo and saddle point techniques (at least, if all particles are pions).

(ii) At lower energies, when only 2, 3, or 4 particle states can contribute, e.g., at the very end of the inclusive x distributions, the FTM is inaccurate.

(iii) Difficulties may arise in the large p_T region ($p_T \gtrsim 4$ GeV), which could, however, be overcome by taking more integration points than we did.

(iv) The method can also be applied to other cutoff functions $f(p_T)$, or other particles than pions.

In a straightforward manner the FTM can be extended to the case of more than one kind of particles. For that purpose one has to compute the different quantities $z(m_i)$ and to construct a new grand partition function Z. Probably the FTM is the most appropriate way to calculate two-particle correlations in the UJM. Since those distributions are of great interest in the study of possible jet structures in many-particle production processes we believe that the FTM will have many applications in the future.

APPENDIX: Two-particle Contributions to the Single-particle Distribution

To take into account the two-particle final state in Eq. (1.4) the sum in Eq. (1.3) has to be supplemented with the $N = 1$ term

$$\kappa\Omega_1(q) = \kappa \int \frac{d^3p_1}{2p_{10}} e^{-\lambda p_{1T}} \delta^{(4)}(p_1 - q), \tag{A.1}$$

so that in Eq. (1.4) we get an extra term

$$F_2(Q, \mathbf{p}) = \kappa^2 e^{-\lambda p_T} \Omega_1(Q - p)/\Omega(Q), \tag{A.2}$$

where

$$\begin{aligned} \Omega_1(Q - p) &= \frac{e^{-\lambda p_T}}{2(s^{1/2} - p_0)} \delta(s^{1/2} - 2p_0) \\ &= \frac{1}{s} e^{-\lambda p_T} \delta(1 - x). \end{aligned} \tag{A.3}$$

Integrating Eq. (A.2) leads, of course, back to the two-particle contribution to $\langle N \rangle$,

$$\langle N \rangle |_{N=2} = \int \frac{d^3p}{2p_0} F_2 = \frac{\kappa^2 \Omega_2(Q)}{\Omega(Q)}. \tag{A.4}$$

From Eq. (A.2) the corresponding contributions to the normalized x, p_T^2, p_L, y, and $\cos\theta$ distributions are then given by

$$\frac{1}{\sigma_{tot}} \frac{d\sigma}{dx}\bigg|_2 = \kappa^2 \delta(1 - x) \frac{\Omega_2(Q)}{\Omega(Q)}; \tag{A.5}$$

$$\frac{1}{\sigma_{tot}} \frac{d\sigma}{dp_T^2}\bigg|_2 = \frac{\pi\kappa^2}{2s^{1/2}\Omega(Q)} \frac{e^{-2\lambda p_T}}{(p_{MAX}^2 - p_T^2)^{1/2}}; \tag{A.6}$$

$$\frac{1}{\sigma_{tot}} \frac{d\sigma}{dy}\bigg|_2 = \frac{\pi\kappa^2}{4\Omega(Q)\cosh^2 y} e^{-2\lambda p_2(y)}; \tag{A.7}$$

$$\frac{1}{\sigma_{tot}} \frac{d\sigma}{dp_L}\bigg|_2 = \frac{\pi\kappa^2}{2s^{1/2}\Omega(Q)} e^{-2\lambda p_2(p_L)}; \tag{A.8}$$

$$\frac{1}{\sigma_{tot}} \frac{d\sigma}{d\cos\theta}\bigg|_2 = \frac{\pi\kappa^2}{2s^{1/2}\Omega(Q)} p_{MAX} e^{-2\lambda p_{MAX} \sin\theta}. \tag{A.9}$$

The two-particle phase-space volume can be calculated either by direct numerical integration

$$\Omega_2(Q) = \frac{\pi p_{MAX}}{s^{1/2}} \int_0^{\pi/2} d\theta \sin\theta e^{-2\lambda p_{MAX} \sin\theta} \tag{A.10}$$

or by evaluation of the series representation [8]

$$\Omega_2(Q) = \frac{\pi p_{\mathrm{MAX}}}{s^{1/2}} \left\{1 + \frac{\pi}{2} [\mathbb{L}_1(2\lambda p_{\mathrm{MAX}}) - I_1(2\lambda p_{\mathrm{MAX}})]\right\}$$

$$= \frac{\pi p_{\mathrm{MAX}}}{2s^{1/2}} \sum_{K=1}^{\infty} \frac{(-1)^{K+1}\, \Gamma(K + \frac{1}{2})}{\Gamma(\frac{3}{2} - K)(\lambda p_{\mathrm{MAX}})^{2K}}. \tag{A.11}$$

REFERENCES

1. J. GASSER, Cambridge University preprint DAMTP 75/22; *J. Math. Phys. (N.Y.)*, to appear.
2. L. VAN HOVE, *Rev. Modern Phys.* **36** (1964), 655; A. KRZYWICKI, *Nuovo Cimento* **32** (1964), 1067; E. H. DE GROOT AND TH. W. RUIJGROOK, *Nucl. Phys. B* **27** (1971), 45; E. H. DE GROOT, *Nucl. Phys.* B **48** (1972), 295.
3. A. BASSETTO, L. SERTORIO, AND M. TOLLER, *Nucl. Phys. B* **34** (1971), 1.
4. R. BAIER, J. ENGELS, H. SATZ, AND K. SCHILLING, *Nuovo Cimento A* **28** (1975), 455.
5. F. JAMES, FOWL, a general Monte Carlo phase-space program, CERN Program Library, 1970, W505.
6. W. KITTEL, L. VAN HOVE, AND W. WOJCIK, *Comput. Phys. Commun.* **1** (1970), 425.
7. K. KAJANTIE AND V. KARIMÄKI, *Ann. Acad. Sci. Fenn. Ser. A VI* (1972), 395; and *Comput. Phys. Commun.* **2** (1971), 207.
8. M. ABRAMOWITZ AND I. A. STEGUN, "Handbook of Mathematical Functions," National Bureau of Standards, Washington, D.C., 1970.
9. W. ROMBERG, *Det. Kong. Norske Videnskabers Selskab Forhandlinger* **28** (1955), 7.
10. J. S. R. CHISHOLM, A. GENZ, AND G. E. ROWLANDS, *J. Computational Phys.* **10** (1972), 284.
11. A. H. STROUD AND D. SECREST, "Gaussian Quadrature Formulas," Series in Automatic Computation IX, Prentice–Hall, Englewood Cliffs, N.J., 1966.

Printed in Belgium